The Plant Cell, Vol. 21: 1592–1606, May 2009, www.plantcell.org © 2009 American Society of Plant Biologists

# Dynamic Behavior of *Arabidopsis* eIF4A-III, Putative Core Protein of Exon Junction Complex: Fast Relocation to Nucleolus and Splicing Speckles under Hypoxia [W]

**O.A. Koroleva,[a,b,1] G. Calder,[a] A.F. Pendle,[a] S.H. Kim,[c,d] D. Lewandowska,[c] C.G. Simpson,[c] I.M. Jones,[b] J.W.S. Brown,[c,e] and P.J. Shaw[a]**

[a] Department of Cell Biology, John Innes Centre, Colney, Norwich NR4 7UH, United Kingdom
[b] School of Biological Sciences, University of Reading, Whiteknights, Reading, RG6 6AS, United Kingdom
[c] Genetics Programme, Scottish Crop Research Institute, Invergowrie, Dundee DD2 5DA, Scotland, United Kingdom
[d] Division of Biosciences and Bioinformatics, College of Natural Science, Myongji University, Yongin, Kyeongki-do 449-728, Korea
[e] Division of Plant Sciences, University of Dundee, Invergowrie, Dundee DD2 5DA, United Kingdom

**Here, we identify the *Arabidopsis thaliana* ortholog of the mammalian DEAD box helicase, eIF4A-III, the putative anchor protein of exon junction complex (EJC) on mRNA. *Arabidopsis* eIF4A-III interacts with an ortholog of the core EJC component, ALY/Ref, and colocalizes with other EJC components, such as Mago, Y14, and RNPS1, suggesting a similar function in EJC assembly to animal eIF4A-III. A green fluorescent protein (GFP)-eIF4A-III fusion protein showed localization to several subnuclear domains: to the nucleoplasm during normal growth and to the nucleolus and splicing speckles in response to hypoxia. Treatment with the respiratory inhibitor sodium azide produced an identical response to the hypoxia stress. Treatment with the proteasome inhibitor MG132 led to accumulation of GFP-eIF4A-III mainly in the nucleolus, suggesting that transition of eIF4A-III between subnuclear domains and/or accumulation in nuclear speckles is controlled by proteolysis-labile factors. As revealed by fluorescence recovery after photobleaching analysis, the nucleoplasmic fraction was highly mobile, while the speckles were the least mobile fractions, and the nucleolar fraction had an intermediate mobility. Sequestration of eIF4A-III into nuclear pools with different mobility is likely to reflect the transcriptional and mRNA processing state of the cell.**

## INTRODUCTION

Production of mRNA for translation involves a series of co- and posttranscriptional steps: capping, splicing, 3′-end cleavage and polyadenylation, mRNA surveillance, association of proteins to form messenger ribonucleoproteins (mRNPs), and export from the nucleus. These steps are coordinated and regulated by molecular interactions between complexes responsible for the various activities (Ares and Proudfoot, 2005). In addition, the architectural organization of the nucleus plays an essential role in gene expression (Lamond and Earnshaw, 1998; Pederson, 1998; Raska et al., 2006). Maintenance of the correct spatial and temporal structure of nuclear compartments is essential for efficient transcription, mRNA processing, and maintenance of genome integrity. The exon junction complex (EJC) links the different aspects of mRNA biogenesis, such as transcription, splicing, export, surveillance, and translation. The parallel elucidation of the function of this nuclear protein complex and its position with respect to nuclear architecture is required to fully understand mRNA biogenesis and how the cell responds to the many physiological processes and growth and environmental stimuli that they encounter.

The EJC is integrally involved in mRNA biogenesis, is deposited on mRNAs as a result of pre-mRNA splicing, determines the export of mRNPs via the nuclear pore complex, and is involved in mRNA surveillance and/or nonsense-mediated mRNA decay (NMD). The EJC contains >20 different proteins, of which eIF4A-III, Y14, Mago, and MLN51 form the tetrameric core of the EJC, which acts as the RNA binding platform anchoring other EJC components to the spliced mRNA (Ballut et al., 2005; Andersen et al., 2006). Human eIF4A-III is also essential for NMD (Shibuya et al., 2004, 2006). Furthermore, an extensive mutational analysis of human eIF4A-III (Shibuya et al., 2006) and a study of the crystal structure of a tetrameric exon junction core complex (Andersen et al., 2006; Bono et al., 2006) resulted in identification of the regions of eIF4A-III that are functionally important for EJC formation, for binding to other EJC components, and for NMD.

The amino acid sequence of eIF4A-III is highly similar to those of the translation initiation factors eIF4A-I and eIF4A-II, two other members of the DEAD box protein family; however, eIF4A-III is functionally distinct from eIF4A-I and eIF4A-II (Li et al., 1999; Chan et al., 2004). The sequence of eIF4A-III is highly conserved between animals and plants (Figure 1). The members of the DEAD box protein

[1] Address correspondence to o.koroleva@reading.ac.uk.
The author responsible for distribution of materials integral to the findings presented in this article in accordance with the policy described in the Instructions for Authors (www.plantcell.org) is: Peter J. Shaw (peter.shaw@bbsrc.ac.uk).
[W] Online version contains Web-only data.
www.plantcell.org/cgi/doi/10.1105/tpc.108.060434

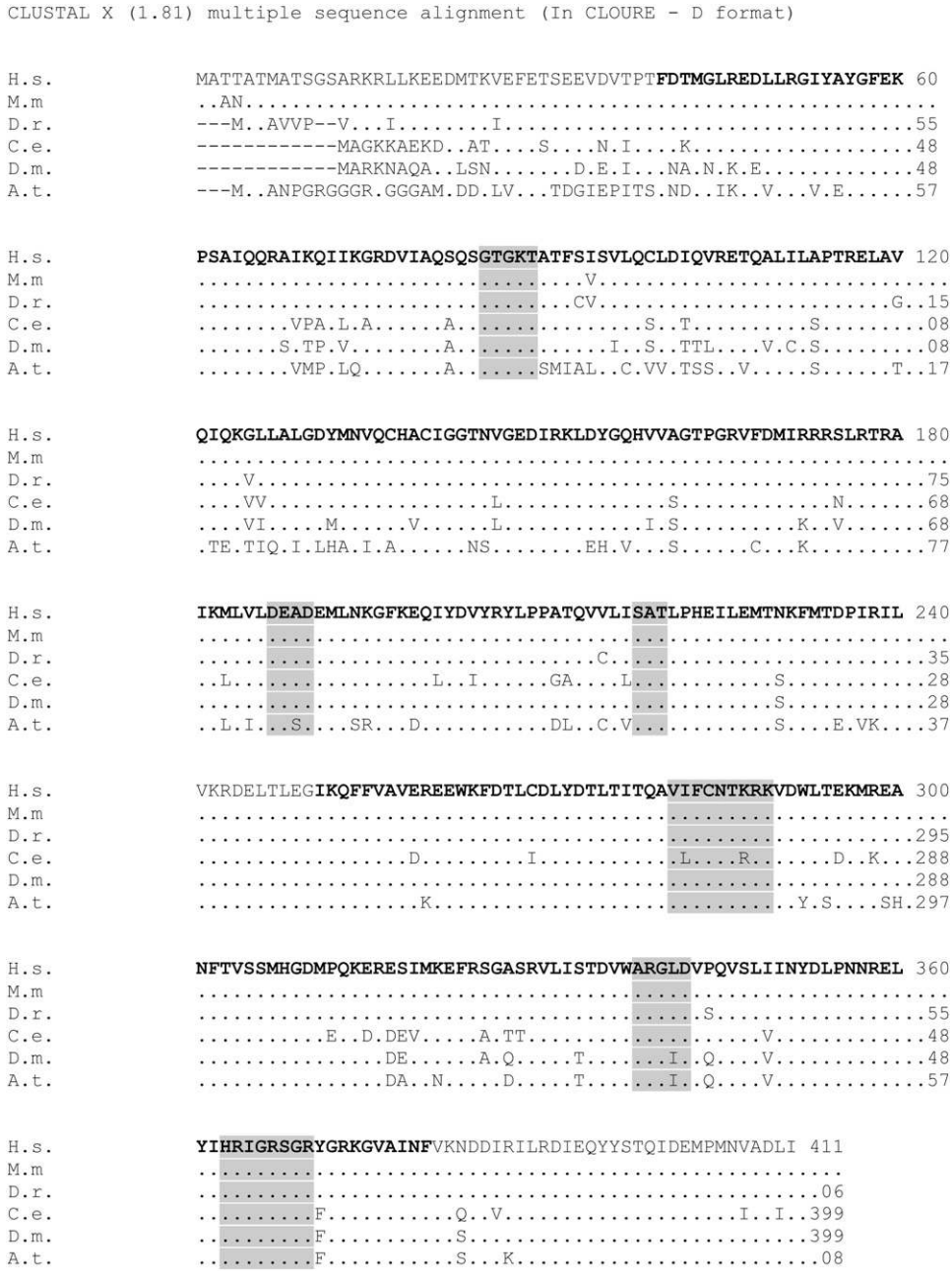


**Figure 1.** Multiple sequence alignment of eIF4A-III.

Multiple ClustalX alignment of *Homo sapiens*, *Mus musculus*, *Drosophila melanogaster*, *Caenorabditis elegans*, *Danio rerio*, and *Arabidopsis* eIF4A-III proteins presented in CLOURE-D format that highlights only the different nucleotides/residues relative to the first query sequence. DEADc (N-terminal) and HELIXc domains (C-terminal) are shown in bold, and functional elements I to VI are shown in boxes.

family are implicated in a number of cellular processes involving alteration of RNA secondary structure, such as translation initiation, nuclear and mitochondrial splicing, and ribosome and spliceosome assembly. Since orthologs of almost all known EJC components have been found in plants (Pendle et al., 2005), it is likely that the plant EJC has a very similar core structure to the mammalian complex.

Proteomic analysis of the plant nucleolus identified six EJC components in the nucleolus, eIF4A-III among them, and the nucleolar association of these and other EJC proteins was confirmed by localization of green fluorescent protein (GFP) fusion proteins (Pendle et al., 2005). The localization of plant EJC factors to the nucleolus was unexpected and suggests that one or more stages of mRNA postsplicing processing, such as mRNA

export, surveillance, or NMD involve the plant nucleolus. Besides the EJC, some splicing factors, including serine/arginine-rich (SR) proteins, were also identified in the nucleolar proteome (Pendle et al., 2005). Recently, the SR protein RSZp22 was shown to localize to the nucleolus under certain conditions most likely reflecting interactions with other proteins (Tillemans et al., 2006).

Here, we show that the identified *Arabidopsis thaliana* eIF4A-III ortholog interacts with *Arabidopsis* ALY-4, a homolog of the mammalian core EJC mRNA export factor Aly/REF. Our data confirm that eIF4A-III is the *Arabidopsis* ortholog of the core EJC factor and that its localization alters under different growth conditions. The subnuclear localization of eIF4A-III is dynamic, as a GFP fusion protein has a general nucleoplasmic distribution under normal growth conditions but localizes to the nucleolus and nuclear splicing speckles under hypoxia stress conditions. The presence and differential dynamic properties of eIF4A-III in these different regions and compartments of the nucleus may reflect different stages of EJC assembly and interactions with mRNA targets.

## RESULTS

### The Protein Sequence of eIF4A-III Is Highly Conserved in Multicellular Eukaryotes

Following its detection in a proteomic analysis of *Arabidopsis* nucleoli (Pendle et al., 2005), we identified the *Arabidopsis* eIF4A-III gene (At3g19760) by a reciprocal BLAST search as the sequence with the highest similarity (e-value 1e-177 and 74% amino acid sequence identity) to the human eIF4A-III gene. DEAD box helicases are a protein family characterized by the conserved motif Asp-Glu-Ala-Asp (DEAD). *Arabidopsis* eIF4A-III was also very similar to an eIF4AIII ortholog previously identified in tobacco (*Nicotiana plumbaginifolia*; Owttrim et al., 1994). A multiple alignment of eukaryotic eIF4A-III sequences reveals highly conserved regions and motifs (Figure 1). *Arabidopsis* eIF4A-III has a DESD motif instead of DEAD as present in animals. All of the conserved motifs of the DEAD box protein family are present in the *Arabidopsis* eIF4A-III protein (Li et al., 1999), such as the ATP binding region I (amino acids 82 to 86); motif II (DESD, amino acids 184 to 187), involved in ATP hydrolysis and coupling ATP hydrolysis to helicase activity; and motif III (SAT, amino acids 215 to 217), critical for RNA unwinding. Motif VI (amino acids 360 to 367) is unique to RNA helicases and is involved in the ATP hydrolysis-dependent RNA binding of eIF4A-III (Li et al., 1999). The multiple alignment indicated that the C-terminal domain is the most conserved part of this protein. This region contains the residues involved in RNA binding and interaction with Mago, Y14, and the Selor domain of MLN51 in the human EJC (Andersen et al., 2006). These residues are among the most conserved residues across different species, suggesting that eIF4A-III forms a core unit of the EJC complex in *Arabidopsis* in a manner similar to the characterized structure of mammalian EJC (Andersen et al., 2006).

### eIF4A-III Interactions with Components of the EJC

#### *Yeast Two-Hybrid Assay*

To examine whether *Arabidopsis* eIF4A-III interacts with EJC core proteins and other EJC components, we screened the interactions of several known orthologs of EJC components in *Arabidopsis*, including eIF4A-III, and two other RNA helicases, translation initiation factors eIF4A-I and eIF4A-II, using a yeast two-hybrid assay. As expected, the strongest reciprocal interaction was observed for proteins Y14 and Mago, as previously shown for animal EJC proteins and in *Arabidopsis* (Park and Muench, 2007). A number of weak interactions were also observed, including eIF4A-III interactions with EJC core proteins Aly1 and Aly4. However, these weak interactions were inconclusive, since they were observed only with eIF4A-III in the pBKT construct. eIF4A-III in the pGADT activation domain construct showed detectable activation with the empty pBKT (see Supplemental Figure 1 online). To further examine these interactions, we undertook a series of pull-down experiments.

### Pull-Down Experiments

Recombinant maltose binding protein (MBP)-eIF4A-III, Y14-GFP, Selor-GFP (Selor domain of MLN51, nucleotides 627 to 863 in open reading frame (ORF) of At1g80000), and Aly4 (At5g37720) proteins were expressed in *Escherichia coli* and purified on Ni columns (all recombinant proteins had a 6xHis tag). Their interaction was tested in vitro using amylose beads to pull-down proteins interacting with MBP-eIF4A-III (Figure 2), either pairwise or in complex mixture of all recombinant proteins. A positive interaction was observed between MBP-eIF4A-III and Aly4, both in pairwise and complex reactions.

### Subcellular Localization of GFP-eIF4A-III

To examine the subcellular localization of eIF4A-III, a translational GFP fusion (GFP-eIF4A-III) was constructed and expressed transiently in *Arabidopsis* Columbia-0 (Col-0) culture cells. GFP-eIF4A-III was found to localize mainly in the nucleus with a small amount of the protein found in the cytoplasm. Nuclear labeling patterns in different cells varied from a diffuse

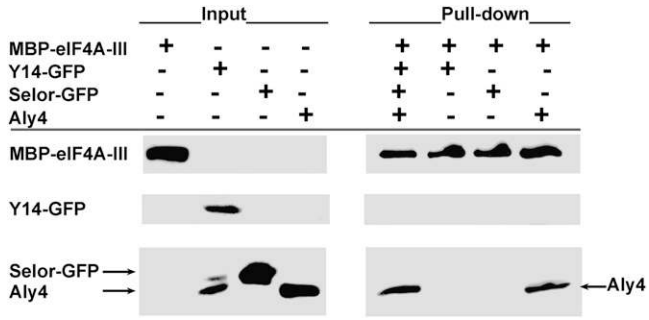


**Figure 2.** Pull-Down Assay Demonstrating Interaction between MBP-eIF4A-III (88 kD) and Aly4-His (30 kD) Proteins, but Not Y14-GFP-His (50 kD) or Selor-GFP-His (37 kD), in Vitro.

Affinity of MBP to amylose was used to pull down MBP-eIF4A-III and associated interacting proteins from the incubation mixture on amylose-conjugated agarose beads. Pull-down products on amylose beads were used for protein gel blot analysis and probed with anti-His-HRP antibodies. Y14-GFP-His degradation products appear in the 32- to 35-kD size range in second input lane.

signal in the nucleoplasm, to concentrated labeling of the nucleolus (Figure 3A to 3C) and speckles (Figure 3B to 3D). Dual localization of GFP-eIF4A-III with several nuclear red fluorescent protein (RFP) fusion marker proteins allowed the identification of the subnuclear compartments (Figure 3). Fibrillarin-RFP colocalized with GFP-eIF4A-III in the nucleolus (Figure 3B). Colocalization of GFP-eIF4A-III with CypRS64-RFP (Cyc64-RFP) and the SR protein RNPS1-RFP, also called SR45 by Ali and Reddy (2006) and Tillemans et al. (2006), confirmed its localization in splicing speckles (Figures 3C and 3D). Splicing speckles are known to be sites for processing, storage, and/or recycling of splicing factors (Lamond and Spector, 2003; Lorkovic and Barta, 2004; Tillemans et al., 2005, 2006). Finally, coilin-RFP, a marker for Cajal bodies (Collier et al., 2006) which are often associated with the nucleolus, did not appear to colocalize with GFP-eIF4A-III (Figure 3A).

To confirm the identification of At3g19760 as the *Arabidopsis* ortholog of mammalian eIF4A-III, we performed colocalization studies with two well-known components of the EJC core complex, Mago and Y14. Complete colocalization in both the nucleolus and speckles was observed for GFP-Y14 and eIF4A-III-RFP (Figure 4A), while GFP-Mago colocalized with eIF4A-III-RFP mainly in the nucleolus and partially in speckles (Figure 4B).

### Dynamics of Localization of GFP-eIF4A-III

The different subnuclear localization patterns observed suggest that eIF4A-III localization changes under different conditions. To examine the dynamics of eIF4A-III localization, we used both transient expression in Col-0 cell cultures and stable transgenic plant lines expressing the GFP-eIF4A-III fusion protein. When

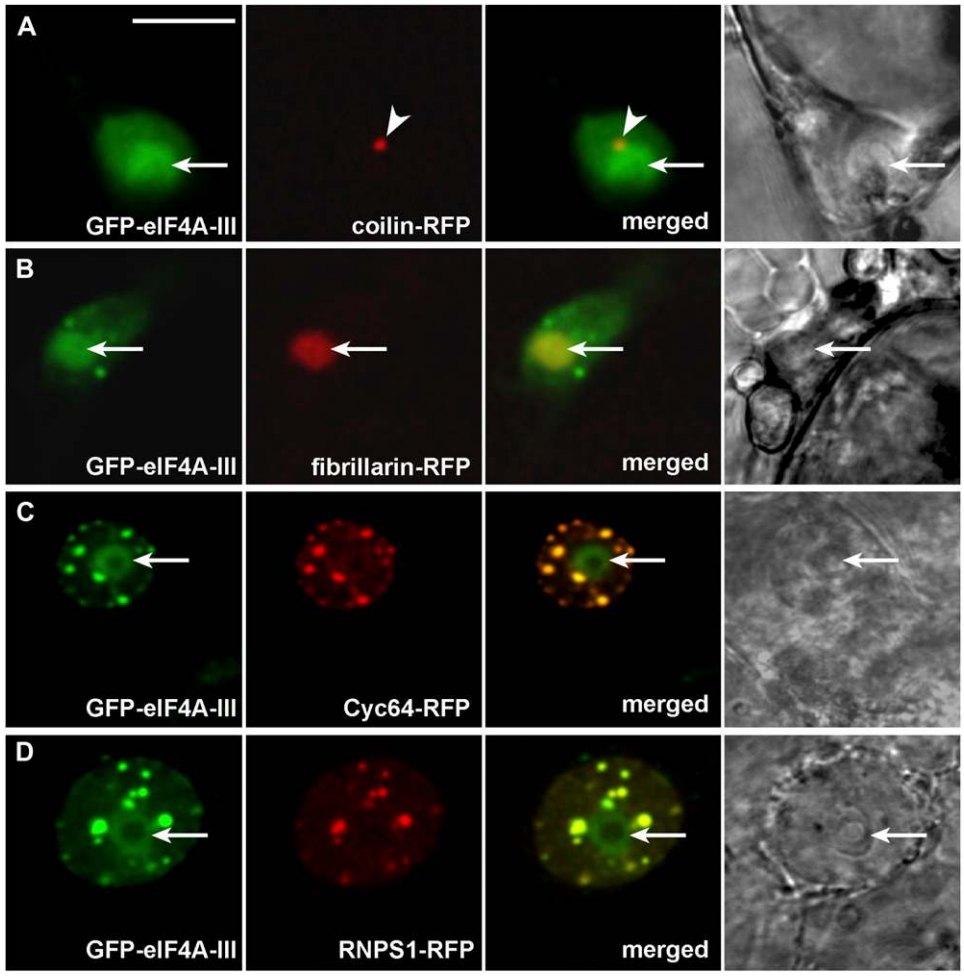


**Figure 3.** Dual-Localization Images of GFP-eIF4A-III with Several Nuclear Marker Proteins.

**(A)** Coilin-RFP (Cajal body).
**(B)** Fibrillarin-RFP (nucleolus).
**(C)** CypRS64-RFP (splicing speckles).
**(D)** RNPS1-RFP (splicing speckles) in Col-0 cells.
Single confocal sections of GFP and RFP channels, merged fluorescent images, and corresponding bright-field images shown. Arrows indicate nucleoli; arrowheads indicate Cajal body. Bar = 10 μm.

*Arabidopsis* Col-0 cells transiently transformed by GFP-eIF4A-III were imaged within 10 to 15 min of taking a sample from culture grown in optimal conditions, the majority of observed cells displayed diffuse fluorescence throughout the nucleoplasm, often with less intensity of signal in the nucleolus (Figures 5, 6, and 8; see Supplemental Figure 2 online). Hypoxic conditions induced by placing culture cells on a microscope slide covered by a cover slip resulted in the relocation and accumulation of the GFP signal into nucleoli and nuclear speckles, usually after 15 to 20 min, with significant fading of the signal in the nucleoplasm (Figure 5; see Supplemental Movie 1 online). Detailed examination of the dynamics showed that GFP-eIF4A-III accumulated first in the nucleolus, immediately followed by the appearance of speckles, usually at the periphery of the nucleolus. The prevalence of nucleoplasmic labeling correlated with optimal grown conditions of the culture cells: continuous shaking at 100 to 150 rpm in flasks or multiwell plates permitting air permeation and an adequate supply of oxygen and temperatures not higher than 25°C.

To follow the dynamic relocalization of GFP-eIF4A-III in more controlled conditions, culture cells were placed in a gas-permeable microscopy chamber in a small volume. Under these conditions (expected to gradually deplete oxygen and/or nutrients), the transition from nucleoplasmic to speckle labeling occurred in a very synchronous manner over a much longer time period (see Supplemental Figure 2 and Supplemental Movie 2 online). The transition of the GFP-eIF4A-III from diffuse nucleoplasmic labeling into nucleoli was observed by 160 min after transfer to the chamber and into speckles in 160 to 220 min. These results clearly demonstrate the pathway of transport of eIF4A-III from nucleoplasm to nucleolus and finally splicing speckles. In addition, this transport pathway was shown to be reversible as closing the gate, and thus restricting gas exchange, caused speckles to appear (more quickly than above) (cf. Figures 6A and 6B), and reopening the gate led to recovery of nucleoplasmic pattern within 30 min (Figure 6C).

In *Arabidopsis* plants stably expressing GFP-eIF4A-III, a very similar response to hypoxia was observed. A primary root placed in a gas-permeable chamber with adequate aeration continued to grow, and the majority of epidermal and cortical cells displayed a diffuse nuclear GFP signal (Figures 7A and 7C; see Supplemental Movie 3 online). When the root was placed in the chamber with no air supply, depletion of oxygen soon caused the transition from diffuse nucleoplasmic labeling to accumulation in splicing speckles (Figures 7B and 7D). This was observed in root cells near the root tip (Figures 7A and 7B) and in the elongation zone (Figures 7C and 7D; see Supplemental Movies 1 to 4 online) of plants expressing GFP-eIF4A-III. Often, differential sensitivity to stress could be observed between epidermal, cortical, and stele root cells as seen by some heterogeneity of labeling (Figure 7B). Again, the change of localization of eIF4A-III from nucleoplasmic labeling to accumulation in speckles was reversible.

Treatment by the respiratory inhibitor sodium azide (Figure 8) had the same effect as hypoxia, resulting in rapid relocation of GFP-eIF4A-III into nucleolus and speckles in seedlings, consistent with the mode of action through the same mechanism of inhibition of respiration. In control cells, eIF4A-III showed nucleoplasmic labeling (Figure 8A) that became distributed between nucleoli and speckles at low concentration (1 mM) of sodium azide (Figure 8B), whereas a higher concentration of the inhibitor (100 mM) caused predominant accumulation of the protein in the nucleolus (Figure 8C). As eIF4A-III is a spliceosomal component and part of the postsplicing EJC, we asked whether the redistribution of GFP-eIF4A-III with azide treatment correlated with a defect in spicing. To test this, we used an RT-PCR splicing system used to measure alternative splicing changes (Simpson

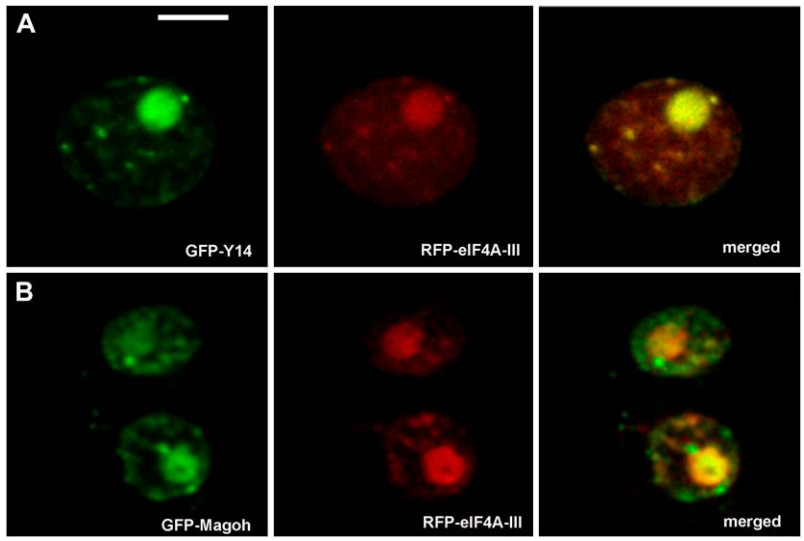


**Figure 4.** Co-localisation of eIF4A-III with Y14 and Mago proteins.

Dual-localization images of eIF4A-III-RFP with GFP-Y14 **(A)** and GFP-Mago **(B)** in Col-0 cells. Single confocal sections of GFP and RFP channels and merged fluorescent images are shown. Bar = 4 μm.

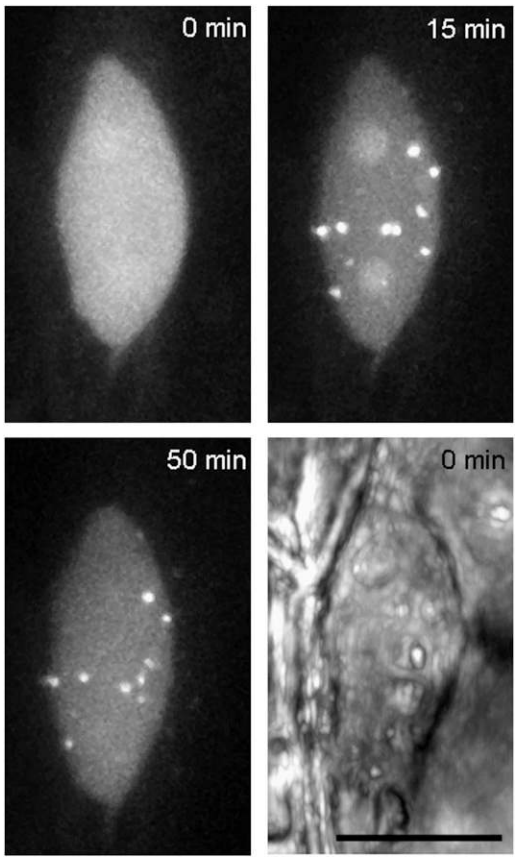


**Figure 5.** Dynamics of Speckle Formation in Nuclei of Col-0 Culture Cells Transiently Expressing GFP-eIF4A-III Placed on a Microscope Glass Slide with a Cover Slip.

Two nucleoli and many bright splicing speckles can be seen at 15 min. The bottom right panel shows a bright-field image of the same nucleus. Bar = 10 μm.

et al., 2008) to examine the splicing of 27 genes that showed evidence of intron retention where an intron is not removed from the transcript. The intron retention events were obtained from plant alternative splicing databases, and the intron retention transcript was detectable with the RT-PCR system (see Methods). We reasoned that if there is a general reduction in splicing, the relative levels of transcripts with unspliced introns would increase. RT-PCR was performed on total RNA prepared from three biological reps of seedlings treated with azide as above and checked for subcellular localization of GFP-eIF4A-III. Following an RT reaction with oligo(dT), the cDNA was aliquoted and PCR reactions with gene-specific primers were performed. Primers were designed to detect all alternatively spliced transcripts in a region and to amplify across more than one intron to distinguish transcripts with an unspliced intron from any signal due to DNA contamination. PCR was performed for 24 cycles (Simpson et al., 2008). The ratio of the amount of fully spliced product to total products (intron retention and fully spliced) was calculated. Of the 27 loci tested for increases in intron retention, 22 showed no effect on splicing, four showed a small increase (>5%) in the relative amount of intron retention transcript compared with fully spliced (see Supplemental Table 1 online; Supplemental Figure 3), and one showed a decrease. Thus, most splicing was unaffected by the treatment such that there was no clear defect that could be associated with the redistribution of GFP-eIF4A-III to speckles or the nucleolus.

### Quantification of Relocalization of GFP-eIF4A-III

Under conditions of low oxygen, GFP-eIF4A-III moved from the nucleoplasm to the nucleolus and then splicing speckles. We quantified this behavior and determined whether other stress conditions or specific inhibitors in culture cells could induce changes in localization. For this purpose, localization of GFP-eIF4A-III was scored as nucleoplasmic (Np), nucleolar (No), nucleolar and speckles (No+S), and speckles (S). Compared with the predominantly diffuse staining of nucleoplasm (85%) in control cells (354 cells and five experiments), the most dramatic and rapid relocation of the GFP-eIF4A-III to the nucleolus and splicing speckles was observed in cells under hypoxia (Table 1) (78% cells with signal in both nucleoli and speckles and 21% with speckles; 102 cells and three experiments). Interestingly, treatment with the proteasome inhibitor MG132 (Table 1) caused a very specific nucleolar accumulation of GFP-eIF4A-III for 48% of cells (338 cells and six experiments). Thus, blocking the proteosome caused the accumulation of *Arabidopsis* eIF4A-III at the intermediate, nucleolar stage in the transport pathway, indicating either that the release of this protein/complex from the nucleolus to the nucleoplasm and/or its accumulation in the splicing speckles requires a proteolysis step or that inhibition of proteolysis enhances a nucleolar sequestration mechanism.

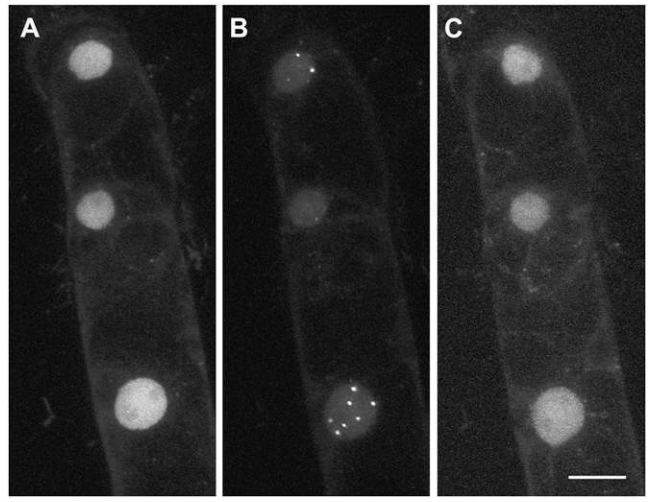


**Figure 6.** Reversible effect of hypoxia treatment on eIF4A-III localisation.

Reversible dynamics of eIF4A-III in transiently expressing Col-0 culture cells placed in a modified gas-permeable chamber with a gate to block gas exchange. Note change from nucleoplasmic location in three nuclei (**[A]**, 0 min) to speckles under hypoxia stress (**[B]**, 60 min) and following recovery to nucleoplasmic pattern after 30 min in aerated conditions (**[C]**, 90 min). Bar = 10 μm.

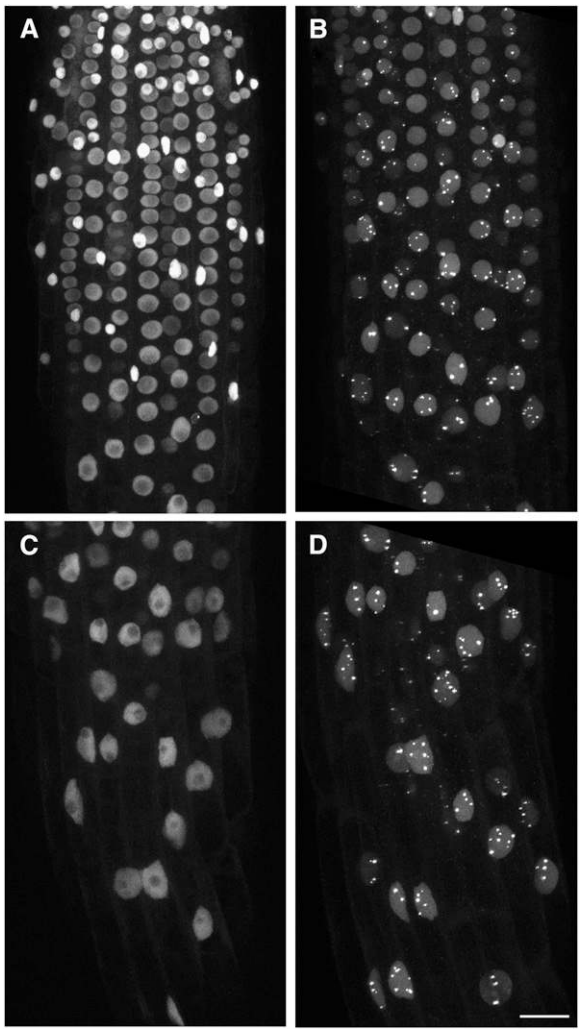


**Figure 7.** Hypoxia caused transition from diffuse nucleoplasmic labelling to accumulation in speckles in nuclei of root cells.

Dynamics of eIF4A-III in *Arabidopsis* roots placed in a gas-permeable chamber: **(A)** and **(C)** with adequate aeration, and **(B)** and **(D)** in hypoxic conditions with 60 min of incubation. **(A)** and **(B)** show an area close to the root tip, and **(C)** and **(D)** show the root elongation zone of the same root. Nucleoplasmic pattern with less signal in the nucleoli can be seen in **(A)** and **(B)**; some nuclei in **(A)** have very intense fluorescence. Faint nucleoplasm with bright speckles can be seen in nuclei in **(B)** and **(D)**. Bar = 10 μm.

### Fluorescence Recovery after Photobleaching Analysis of Intranuclear Mobility of GFP-eIF4A-III

To see whether the properties of *Arabidopsis* eIF4A-III differed among the different regions of the nucleus, we analyzed the mobility of the three different pools of GFP-eIF4A-III (diffuse nucleoplasmic, nucleolar, and splicing speckles) using fluorescence recovery after photobleaching (FRAP). This was performed in both *Arabidopsis* Col-0 culture cells transiently expressing GFP-eIF4A-III and in stably transformed *Arabidopsis* plants. A background fluorescence image was recorded, followed by photobleaching to significantly reduce the fluorescence intensity in a small circle with a diameter of 3 μm (7 $\mu m^2$ area), and the rate of fluorescence recovery was measured as unbleached molecules diffused into the bleached area. Typical FRAP experiments performed on nucleoplasmic, nucleolar, and speckle fractions are shown in Supplemental Movies 5 to 7 online.

Average values of background-normalized recovery data for nucleoplasm, nucleolus, and speckles from 10 independent experiments for each subnuclear compartment in suspension culture cells clearly demonstrated different recovery rates for the three regions (Figure 9A, Table 2). In general, all fractions had recovered to stable values of >75% of the initial fluorescence values within 50 s. Recovery of the nucleoplasmic fraction was the fastest with a half-time of 0.37 s; the splicing speckles required longest times for recovery, with a half-time of 2.89 s; and the nucleolar fraction had an intermediate rate of recovery, with a half-time of 1.54 s. Therefore, the nucleoplasmic fraction represents the most mobile form of GFP-eIF4A-III, the speckles represent the least mobile fraction, and the nucleolar fraction has a mobility that is slightly lower than the nucleoplasm, but still higher than speckles. The maximal level of recovery, as indicated by coefficient a in Table 2, was observed for the nucleoplasmic fraction (86% of the initial value), with a similar level for nucleolar (87%) and a slightly lower value for speckles (80%).

The FRAP data obtained on hypocotyls and root cells of *Arabidopsis* plants also demonstrated consistent differences in mobility between nucleoplasmic and speckle fractions (Figures 9B and 9C). The half-time of fluorescence recovery in nucleoplasmic fractions in *Arabidopsis* plants was very similar to the values from the suspension cells (Table 2) with 0.41 s in hypocotyls and 0.47 s root cells of control plants. As in culture cells, speckles were formed under hypoxic conditions and the mobility of the GFP-eIF4A-III after sequestration to speckles significantly decreased. Fluorescence recovery in the speckles of hypoxia-stressed plants was much slower than in the nucleoplasm, with half-times of 1.30 and 1.60 s in hypocotyls and roots, respectively. Compared with the culture cells, many fewer nuclei with nucleolar concentration of labeling were observed in plant roots stressed with hypoxia; thus, we did not perform FRAP analysis on this compartment in plants. Overall, in both cell culture and whole plants, the half-time of recovery was several times longer for splicing speckles compared with the nucleoplasmic fraction of GFP-eIF4A-III.

## DISCUSSION

### At3g19760 Is the *Arabidopsis* Ortholog of eIF4A-III

The motivation for this study was our finding by proteomics of a number of unexpected proteins in the nucleolar fraction, including putative EJC components (Pendle et al., 2005). We therefore chose eIF4A-III, one of the proteins identified in the nucleolar complement, as a representative EJC core component for detailed analysis. We first confirmed that the identified gene (At3g1970) had the highest similarity to the animal eIF4A-III and showed conservation of the important domains.

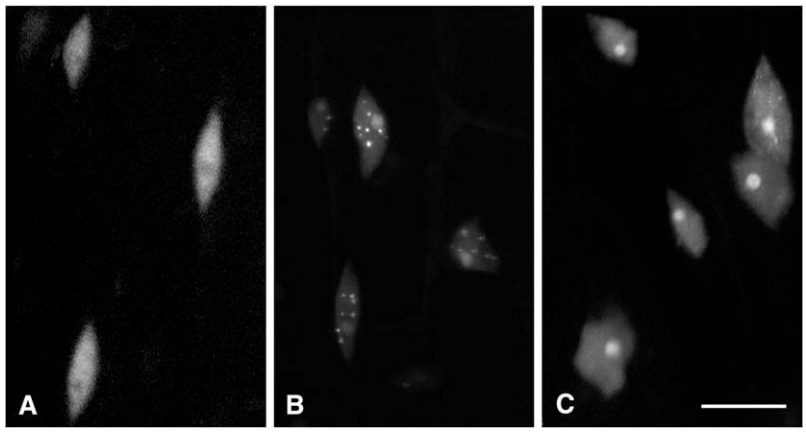


**Figure 8.** The Effect of Inhibition of Respiration by Azide on Localization of eIF4A-III in Hypocotyl Cells Expressing GFP-eIF4A-III.

**C**ontrol cells **(A)**, 1 mM azide **(B)**, and 100 mM azide **(C)** treatment for 30 min. Nucleoplasmic labeling in control cells **(A)** changed to accumulation in nucleoli and speckles at low concentration (1 mM) of sodium azide **(B)**, while a higher concentration of the azide (100 mM) caused predominant accumulation of the protein in the nucleoli **(C)**. Bar = 100 μm.

Our in vitro experiments of MBP-eIF4A-III pull downs with recombinant proteins Y14, Aly4, and the Selor domain of MLN51 detected interaction between MBP- eIF4A-III and Aly4. Very similar results were obtained in the original article by Chan et al. (2004) (which identified human eIF4A-III as a novel component of the EJC) that recombinant GST-eIF4A-III only bound to Aly/Ref and TAP proteins but did not significantly bind to the EJC components Mago, Y14 (binding <2%), Upf3a, RNPS1, UAP56, or SRm160. These results suggested that human eIF4A-III associates with Y14 and Mago indirectly through its interaction with TAP and Aly/REF, which were identified as positive interactions in a pull-down assay (Chan et al., 2004).

The absence of strong interactions of eIF4A-III in yeast two-hybrid assays is probably due to the fact that EJC complex assembly is known to depend on the presence of spliced mRNA, in which eIF4A-III retains bound ATP, and the fact that the interactions within the complex are likely to be mediated by ternary interactions between the components. It has been shown in mammalian cells that the EJC is stabilized and locked onto RNA by inhibition of eIF4A-III ATPase activity (Ballut et al., 2005), and it is very likely that the complex dissociates in the absence of mRNA. The low abundance of the EJC proteins and transient and labile nature of this complex present substantial obstacles for isolation of the complex from plants and may explain low success in identification of interactions in yeast two-hybrid and tap-tag pull-down experiments (Park and Muench, 2007).

We further analyzed the EJC complex components by in vivo colocalization studies. Complete colocalization in both nucleolus and speckles was observed for GFP-Y14 and eIF4A-III-RFP (Figure 4A), while GFP-Mago colocalized with eIF4A-III-RFP mainly in the nucleolus and only partially in speckles (Figure 4B). Colocalization of *Arabidopsis* Y14 and Mago proteins with a marker for nuclear speckles SRp34 has been previously demonstrated (Park and Muench, 2007), and nucleolar localization was confirmed by both proteomic studies and transient expression of GFP fusions (Pendle et al., 2005). The nuclear localization is a unique feature of eIF4A-III, since RNA helicase with high sequence similarity, eIF4AI, is predominantly cytoplasmic (Dhalia et al., 2006) like some other proteins from the same family (Koroleva et al., 2005). Thus, various lines of evidence confirm that At3g19760 is the *Arabidopsis* eIF4A-III ortholog, and we refer to it subsequently as eIF4A-III.

### *Arabidopsis* eIF4A-III Is Highly Dynamic and Is Localized in the Nucleolus as well as the Nucleoplasm and Splicing Speckles

Initial microscopic observation using *Arabidopsis* cells transformed with GFP-eIF4A-III showed that the tagged protein was localized to three different subnuclear locations: the nucleoplasm, the nucleolus, and nuclear speckles. The speckles were identified as splicing speckles by colocalization with CypRS64 and the SR protein RNPS1/SR45 RFP fusion markers, and the nucleolar location was confirmed by colocalization with a fibrillarin-RFP fusion marker. However, further analysis revealed that GFP-eIF4A-III localization was highly dynamic and very sensitive to cellular conditions. Under optimal conditions, it was distributed

**Table 1.** Distribution of Localization Patterns of eIF4A-III Observed in Cells Treated with MG132 or Hypoxia Compared with Control Cells

| | Expressing Cells [% (number of cells)] | | | | |
|---|---|---|---|---|---|
| Treatment | N | No | No+S | S | Total Cells |
| Control | 85.0 (301) | 13.6 (48) | 0.8 (3) | 0.6 (2) | 100 (354) |
| MG132 (100 μM) | 51.5 (174) | 48.2 (163) | 0 (0) | 0.3 (1) | 100 (338) |
| Hypoxia (20 min) | 0 (0) | 1.0 (1) | 78.4 (80) | 20.6 (21) | 100 (102) |

Each column presents percentage (number) of cells with a specific pattern of localization: N, diffuse nucleoplasm; No, nucleoli; No+S, nucleoli and nucleoplasmic speckles; and S, speckles.

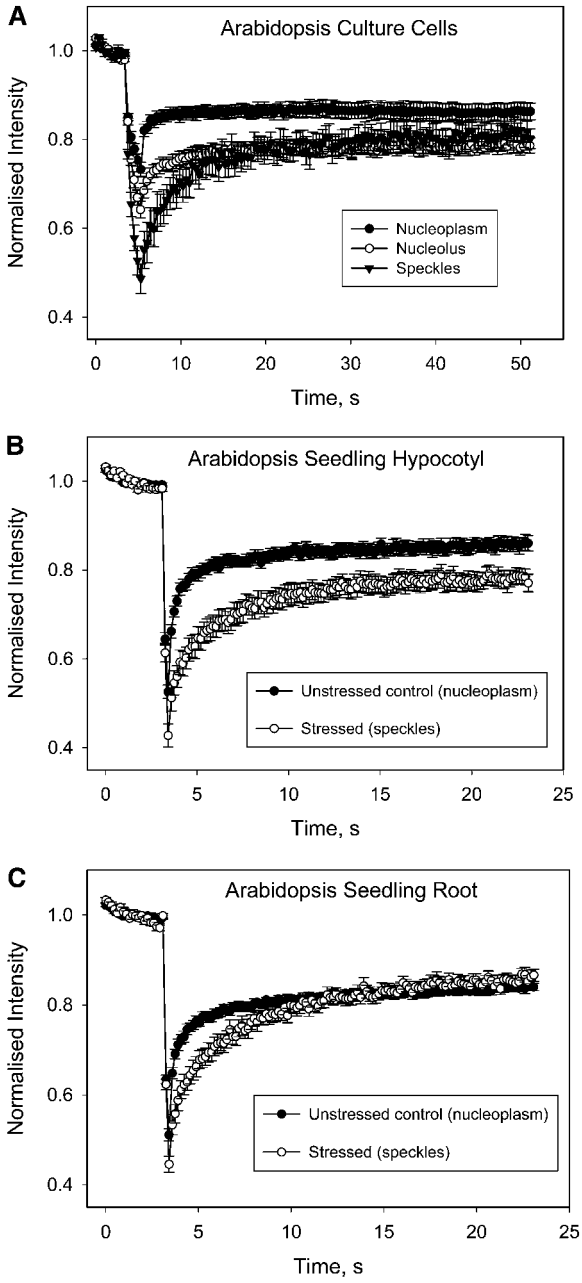


**Figure 9.** Intranuclear Mobility of Different Pools of GFP-eIF4A-III and FRAP Analysis of Different Nuclear Fractions.

The background fluorescence was recorded, followed by photobleaching to significantly reduce the fluorescence intensity, and the fluorescence recovery was recorded as unbleached molecules diffused into the bleached area. Each line plotted using mean values ± SE of 10 individual experiments. Formal kinetic parameters of recovery (maximal recovery, rate constant, and recovery half-time) were estimated using exponential model curves based on equation of one-phase exponential formation/association.

**(A)** Diffuse nucleoplasmic, nucleolar, and speckles fractions in culture cells transiently expressing GFP-eIF4A-III.

**(B)** Nucleoplasmic and speckles fractions of GFP-eIF4A-III in control and stressed hypocotyl cells of stably transformed *Arabidopsis* plants.

**(C)** Nucleoplasmic and speckles fractions of GFP-eIF4A-III in control and stressed root cells of stably transformed *Arabidopsis* plants.

throughout the nucleus, but under conditions of hypoxia, it relocated in a matter of minutes to the nuclear speckles, often showing a temporary intermediate accumulation in the nucleolus. These results were closely paralleled by the behavior of GFP-eIF4A-III in seedlings of a stable transformed line expressing the fusion protein. We confirmed that the inhibition of respiration is the primary cause of relocation of the protein to the nucleolus and speckles under hypoxic conditions by showing that sodium azide had the same effect as hypoxia in seedlings.

A thorough study of the localization and dynamics of another component of the EJC complex, RNPS1/SR45, found that it was dependent on ATP, phosphorylation, and transcription (Ali and Reddy, 2006). These authors found GFP-SR45 both in speckles (which exhibited intranuclear movements and changes in morphology) and the nucleoplasm in interphase nuclei. Inhibition of transcription and protein phosphorylation resulted in redistribution of SR45 to larger speckles. The nuclear speckles correspond to interchromatin granule clusters and probably serve as the storage/recycling sites for splicing factors, delivering the splicing factors to the nearby active sites of transcription (Misteli and Spector, 1998; Misteli, 2005). Since we found that eIF4A-III and RNPS1/SR45 always simultaneously colocalize in the nuclear speckles under hypoxia treatment, it is most likely that these two proteins (and probably several other components of the EJC) are subject to coordinated relocation in response to a change in transcription rate. Interestingly, splicing was largely unaffected in cells where eIF4A-III was localized in the nucleoplasm, speckles, and nucleolus due to azide treatment, although small increases in transcripts with unspliced introns were detected for some genes analyzed. Therefore, it is likely that under the conditions used, a general reduction in splicing is not yet apparent and the observed changes in relocalization reflect either unbound eIF4A-III or eIF4A-III bound to spliced mRNAs.

On the other hand, treatment of the cells with the proteasome inhibitor MG132 caused a significant increase in the number of cells with a marked concentration of the protein in the nucleolus and virtually no cells with localization to speckles. Thus, the proteasome inhibitor altered the relocalization pathway, again suggesting that relocalization of eIF4A-III from the nucleoplasm to speckles involved an intermediate localization in the nucleolus.

Other investigators analyzing SR splicing factors have observed similar behavior. For example, Tillemans et al. (2006) showed in transiently transformed *Arabidopsis* that GFP-RSZp22 is localized predominantly to speckles but also to the nucleolus. Expression of a series of deletion constructs demonstrated that the nucleolar localization depended on a number of protein domains rather than on a single nucleolar targeting signal. This agrees with the general conclusion that proteins locate to the nucleolus as a result of the interactions they form in complexes with other proteins (Shaw and Jordan, 1995; Raska et al., 2006). Furthermore, a general picture is emerging in which many, if not all, nuclear and nucleolar proteins are highly dynamic, diffusing throughout the nuclear volume; their concentration in particular subnuclear regions or bodies, such as the

**Table 2.** FRAP Parameters Estimated for Different Nuclear Fractions of GFP-eIF4A-III Using Curve-Fitting Software TableCurve2D

| | | | | Hypocotyl Cells | | Root Cells | |
|---|---|---|---|---|---|---|---|
| | Culture Cells | | | Control | Hypoxia | Control | Hypoxia |
| Parameter | Nucleoplasm | Nucleolus | Speckle | Nucleoplasm | Speckle | Nucleoplasm | Speckle |
| **a**, Max recovery, decimal fraction ± SE | **0.863** | **0.873** | **0.799** | **0.842** | **0.767** | **0.820** | **0.837** |
| | 0.000 | 0.001 | 0.002 | 0.002 | 0.002 | 0.002 | 0.003 |
| **b**, rate constant, $s^{-1}$ ± SE | **1.860** | **0.450** | **0.240** | **1.701** | **0.535** | **1.462** | **0.432** |
| | 0.110 | 0.020 | 0.008 | 0.092 | 0.019 | 0.087 | 0.016 |
| $\mathbf{T_{1/2}}$, recovery half -time, s | **0.373** | **1.540** | **2.892** | **0.407** | **1.295** | **0.474** | **1.604** |
| $\mathbf{R^2}$, correlation coefficient | 0.892 | 0.889 | 0.936 | 0.859 | 0.917 | 0.817 | 0.919 |

nucleolus and speckles, is determined by differential retention and thus different residence times in the different compartments, reflecting interactions with other proteins or complexes (Carmo-Fonseca et al., 2000; Lamond and Spector, 2003).

### FRAP Data Suggest Different Complexes in the Three Locations

We used FRAP to study further the dynamics of GFP-eIF4A-III. In contrast with FRAP studies of GFP-RSZp22 by Tillemans et al. (2006), who found similar rates of recovery in the nucleoplasm, nucleolus, and speckles, we demonstrated very different recovery times in the three compartments. The diffuse nucleoplasmic distribution was the most dynamic with a recovery half-time of ~0.5 s, the nucleolar recovery was slower at ~1 s, and the speckle recovery was the slowest at ~2 s. The simplest interpretation of our results is that the eIF4A-III is involved in at least three different types of complex, corresponding to the different locations.

The EJC contains proteins that are recruited as part of the spliceosome, that interact with mRNP export adaptors, that enhance translation, or that are involved in NMD (Stutz and Izaurralde, 2003; Maquat, 2004; Tange et al., 2004; Lejeune and Maquat, 2005; Andersen et al., 2006). As such, EJC proteins link gene transcription with splicing, export, translation, and NMD and are present in a number of different biochemical forms in the nucleus. These include association with nascent transcripts, released unspliced and spliced mRNP complexes, and mRNP complexes undergoing export, translation, and NMD. It is also likely that there is a population, perhaps the major fraction, of these proteins that are not bound in RNP complexes. However, there are little or no data on the relative amounts of these different types of complex. Although it is not possible from our results to determine the nature of the complexes underlying our microscopy observations and which, if any, represent RNP complexes, the different localizations and FRAP dynamics are indicative of eIF4A-III existing in different complexes that govern their subnuclear localization. The same considerations apply to the previous observations by others of the SR proteins and to the native proteins as well as GFP fusion proteins. To confidently observe the dynamics of the RNP complexes, it will be necessary to use a specific fluorescently tagged RNA and probably moreover to image the RNA fraction bound to a specific tagged protein using Fluorescence Resonance Energy Transfer (FRET) or bimolecular fluorescence (Rackham and Brown, 2004).

Even bearing in mind the foregoing reservations, the diffuse nuclear localization, in which the protein is neither concentrated nor excluded from the speckles and the nucleolus, must represent the optimal cellular state, with active transcription and splicing. Splicing speckles have been widely considered to represent a store of spliceosomal precursor complexes, which are recruited to transcription/splicing complexes under conditions of active transcription but accumulate in splicing speckles when transcription is suppressed. In agreement with this, the hypoxia treatment is likely to severely repress transcription, splicing, or both and causes redistribution from the nucleoplasm and nucleolus to the speckles. However, it is important to note that speckles are not simply end-point storage sites but are in rapid equilibrium with the rest of the nucleus (Carmo-Fonseca et al., 2000); an inert accumulation of proteins would be permanently photobleached and would not recover. This is also the case for the eIF4A-III complexes in plant speckles, which from our data have a FRAP recovery half-time only a factor of ~4 times greater than the nucleoplasmic fraction.

The redistribution of eIF4A-III first to the nucleolus prior to speckles is intriguing as the nucleolus is not usually thought to be associated with mRNAs or mRNPs. However, cellular stresses cause relocalization of particular proteins, such as heat shock and some RNA binding proteins, to the nucleolus, which are thought to act as chaperones for proteins and RNPs (Alastalo et al., 2003; Segui-Simarro et al., 2003). Removal of the stress reverses the process and releases the RNPs. Other studies have shown that many RNA binding proteins localize to the nucleolus or to nucleolar caps on inhibition of transcription (Shav-Tal and Singer, 2005). Thus, the initial accumulation of eIF4A-III in the nucleolus may represent an early response to the stress conditions reflecting the sequestration of mRNPs in different stages of maturation. The subsequent relocalization to speckles may represent a later response to the continued stress conditions where mRNP complexes are turned over by releasing RNP components, including EJC complexes (which then move to speckles), and degrading the mRNA. The nucleolar accumulation of eIF4A-III after proteasomal inhibition with MG132 is particularly interesting in this respect and suggests that proteolysis may be involved in turning over the complexes containing eIF4A-III. Recently, Baldin et al. (2008) identified

proteasome-PA28γ complexes as a novel regulator of nuclear speckles organization and function, acting most likely through selective proteolysis. This step is likely to be necessary for the normal equilibrium between the different nuclear compartments, and in the absence of this putative proteolysis, the resulting complex has a great affinity for or residence time in the nucleolus.

### What Is the Mechanism of Rapid Relocation of eIF4AIII to Nucleolus and Splicing Speckles in Response to Hypoxia?

The most rapid and dramatic relocalization of the eIF4A-III protein was observed as a reaction to hypoxic conditions, also seen in response to treatment by sodium azide. Hypoxic conditions bring about a very rapid depletion of the ATP pool. Suppression of major energy-consuming processes in cells provides protection against hypoxia, and one of the first consequences of hypoxia treatment on cell functions is a rapid inhibition of protein synthesis. Hypoxia-tolerant animal cells experience a 90% or greater global decline in both protein synthesis and degradation (Hochachka et al., 1996). Similarly, in plant tissue (potato tubers), low internal oxygen concentrations led to the rates of protein synthesis decreased to <10% of their values at ambient oxygen (Geigenberger, 2003). A hypoxia-induced block of protein synthesis could occur either at the level of gene transcription or translation , at both initiation and elongation stages.

The experimental evidence available in plant cells suggests inhibition of protein synthesis at the elongation step via formation of nonfunctional complexes of elongation factor with polysome-associated mRNA (Vayda et al., 1995) and selective repression of translation achieved via adjustments in the levels of polyribosomes (Branco-Price et al., 2008). Moreover, upon oxygen deprivation, the majority of the translationally impaired mRNAs become stabilized in nonpolysomal complexes and they can be rapidly recruited to polysomes upon reoxygenation, thus enhancing conservation of energy by minimization of the need for de novo transcription upon reoxygenation (Branco-Price et al., 2008). However, it is still not known how cells recognize the correct moment to turn on their hypoxia defense mechanisms (Bailey-Serres and Chang, 2005), and our work may provide an insight into early stages of direct oxygen sensing, which precedes (and most likely controls) any changes in translational activity.

A recent study in mammalian cells linked the EJC to translational control. It has been found that the EJC activates translation downstream of the mTOR signaling pathway (involved in nutrient sensing) via SKAR-mediated recruitment of activated S6K1 to newly processed mRNPs and thus increasing the translation efficiency of spliced mRNA in a pioneer round of translation (Ma et al., 2008). The DEAD box protein eIF4A-III is an ATPase itself, which might provide a direct link between ATP/ADP status in a cell in hypoxic conditions and eIF4A-III localization and function. Studies of crystal structure of the EJC core showed that eIF4A-III encloses an ATP molecule, which changes its conformation and provides the binding sites for ribonucleotides. A network of interactions anchors Mago, Y14, and MLN51 at the interface between the two domains of eIF4A-III, effectively stabilizing the ATP bound state and locks the complex on the mRNA (Andersen et al., 2006; Bono et al., 2006). The ATP-bound form of the eIF4AIII-MLN51 complex has a 100-fold higher affinity for RNA than the unbound form, and ATP hydrolysis reduces this affinity (Noble and Song, 2007). In the conditions of ATP deficiency, most of the eIF4A-III protein will not enclose an ATP molecule and therefore not have a conformation that allows it to assemble on mRNA substrate. The change in the conformation of eIF4A-III protein without bound ATP might be a signal for its sequestration for storage/processing. The function of eIF4A-III will also be affected by the repression of transcription and/or splicing under hypoxia reducing the levels of nascent, processed, and mature mRNAs requiring assembly of EJCs and thereby the number of nucleoplasmic binding sites for eIF4A-III, again likely to promote relocation to speckles for storage.

## METHODS

### Sequence Analysis of eIF4AIII

Multiple sequence alignment of *Homo sapiens*, *Mus musculus*, *Drosophila melanogaster*, *Caenorabditis elegans*, *Danio rerio*, and *Arabidopsis thaliana* eIF4AIII proteins was performed using ClustalX program and reformatting the output data using CLOURE (Clustal Output Reformatter; Kohli and Bachhawat, 2003) in a format that highlights only the different nucleotides/residues relative to the first query sequence.

### Construction of GFP and RFP Protein Fusions and Expression in Plant Cells

A full-length ORF of eIF4A-III (At3g19760) was PCR amplified (with removed stop codon) from the cDNA library and inserted into pDONR207 vector (Invitrogen). The GFP fusion construct was made using Gateway recombinational cloning into GFP-N-Bin expression vector as previously described (Koroleva et al., 2005). ORFs of known marker proteins RNPS1/SR45 (splicing speckles) and FIBRILLARIN1 (nucleolus) were PCR amplified from cDNA and cloned into pDONR207 vector; the ORF of CypRS64 (splicing speckles) was amplified from pCypRS64-GFP plasmid (Lorkovic et al., 2004), and pDONR207 coilin (Cajal body) was as described by Collier et al. (2006) and GFP-Y14 as described by Pendle et al. (2005). Construction of RFP fusions of marker proteins was performed using LR reaction for recombination between pDONR207 clones containing appropriate ORFs and a Gateway-compatible vector pROK2-mRFP, which contains coding sequence of monomeric RFP (Campbell et al., 2002) at the C-terminal end of the AttR cassette.

The constructs were transiently expressed in Col-0 *Arabidopsis* cell culture as previously described (Koroleva et al., 2005). Briefly, Col-0 suspension culture was diluted 1:5 with fresh AT media (4.4 g/L Murashige and Skoog [MS] salts, 3% sucrose, 0.05 mg $L^{-1}$ kinetin, and 0.5 mg $L^{-1}$ naphthalene acetic acid (NAA), pH 5.8) and transformed by coculture with *Agrobacterium tumefaciens* carrying expression vector, for 3 to 5 d in the dark conditions at 25°C with shaking (150 rpm) and good aeration.

*Arabidopsis* plants (Col-0 ecotype) were transformed by the floral dip method (Clough and Bent, 1998), and T1 seedlings selected on Petri plates with MS-agar media containing 50 μg/L kanamycin. Kanamycin-resistant seedlings expressing a moderate level of GFP-eIF4A-III were further selected using fluorescence microscopy. The seedlings were grown vertical on MS-agar plates in a growth room under constant light at 25°C. The localization patterns were consistent between several lines in T1 and T2 generations.

### Yeast Two-Hybrid Assays

Full-length ORFs of the components of the *Arabidopsis* EJC (Pendle et al., 2005; or amplified as described above using PCR primers in

Supplemental Table 2 online) in pDONR207 were used in recombination reactions to transfer genes to pDEST-GADT7 and pDEST-GBKT7 vectors (Rossignol et al., 2007). GADT7 products were transformed into *S. cerevisiae* strain AH109 and GBKT7 products into strain Y187 (Matchmaker III; Clontech Laboratories).

After pairwise mating of strains expressing the EJC constructs, colonies were grown on media depleted of Leu, Trp, His, and adenine or on media depleted of Leu and Trp containing X-α-galactose. Yeast strains transformed by empty vectors and pLam5 were used as negative controls and T-antigen with p53 as a positive control.

### Recombinant Protein Purification and Pull-Down Assays

ORFs of eIF4A-III, Y14, the Selor domain of MLN51 (At1g80000, nucleotides 627 to 863), and ALY4 (At5g37720) were amplified with PCR primers (see Supplemental Table 2 online), digested by *Sfi*I, and cloned into pTriEx-SfiI vectors (Pengelley et al., 2006) for translational fusion to MBP or GFP; all vectors also contained the 6xHis tag. Recombinant proteins were expressed in *Escherichia coli* and purified on His-Trap Ni sepharose columns (GE Healthcare). Their interaction was tested in vitro, either pairwise or in complex mixture of all recombinant proteins. Protein mixtures containing MBP-eIF4A-III were incubated in 1.5 mL of binding buffer (20 mM Tris-HCl, 0.2 M NaCl, 0.1% Nonidet P-40, and 5% glycerol, pH 7.4) for 2 h at 4°C and gentle rotation; then 30 μL of amylose beads (New England Biolabs) were added, followed by additional incubation for 1 h. The amylose beads were washed three times with binding buffer and bound proteins eluted with SDS sample buffer. Eluted proteins were separated on 10% SDS polyacrylamide gels and used for protein gel blotting with anti-His-HRP antibodies (Roche). Pull-down experiments were repeated twice.

### Confocal Microscopy Imaging of Dual Localization of GFP and RFP Protein Fusions

Col-0 cells in exponential phase of the culture (within 2 to 5 d of subculturing in fresh media) transiently expressing GFP-eIF4A-III with a selected marker protein-mRFP fusion were imaged using Leica SP and SP2 laser scanning microscopes with a ×40 oil immersion objective. The fluorescent images of cells expressing both reporters were taken at 512 × 512 pixels resolution (pixel size ranged from 2 to 60 $nm^2$) using combinational excitation of 80% of laser power at 488 nm and 20% of laser power at 543 nm, and detection windows of 500 to 550 and 630 to 680 nm for GFP and RFP channels, respectively. Images of averaged intensity of three to four scans were collected.

### Time-Lapse Confocal Microscopy and Analysis

*Arabidopsis* cells, either Col-0 culture or roots of plants transformed with GFP-eIF4A-III, were imaged using either a Leica SP1 or SP2 confocal microscope (Leica Microsystems). GFP was excited using 488-nm light from an argon ion laser and imaged using emission filters 505 to 555 nm. At each time point, a z-stack of images (with a 1- to 2-μm z-step) was collected, and the images from z sections were projected using the maximum intensity projection algorithm in either the Leica software or ImageJ program (http://rsb.info.nih.gov/ij/). Time-lapse imaging of living cells was acquired at 3- to 20-min intervals, in a gas-permeable biochamber.

The biochamber was constructed from a standard cover slip (number 1.5, 50 × 22 mm) as the top (viewing part) of the chamber. A well (~16 × 24 mm) was made in Secure Seal (double-sided adhesive sheet; Grace Bio-Labs) and attached to the cover slip. The plant was placed in the well with liquid MS media, and a gas-permeable membrane (BioFolie; Viva Science) was attached to the Secure Seal as the bottom of the chamber. The chamber was then mounted on a support slide to allow normal attachment to any microscope; an 18-mm-diameter hole was cut in this support slide to allow free gaseous exchange through the gas-permeable membrane.

For the reversible hypoxia experiment, the biochamber was modified to allow gating of the membrane. Each end of the biochamber was raised by two cover slips (22 × 22 mm) before being attached to the support slide. A third cover slip, 22 × 50 mm, was positioned between the two cover slips so that it could slide over the hole, like shutting a gate. This gating cover slip is not sufficient to block gaseous exchange by itself; water had to be added between the membrane and the gating cover slip to block gaseous exchange. Water was used instead of oil to allow the process to be reversed.

Seedlings (3 to 5 d old) or cells (2 to 5 d after subculturing in fresh media) were then placed into the chamber and covered with a gas-permeable membrane. The chamber with the gas-permeable membrane facing down was then placed over a 1-cm hole drilled into a plastic support slide and the edges of the sandwich sealed with tape.

### Stress and Recovery Experiments

Plants and cells were imaged using a Zeiss 510 Meta confocal microscope (Carl Zeiss Microimaging) using a ×40 objective. GFP was exciting using the 488-nm laser line from an argon ion laser, and the emission was captured using a 505- to 550-nm band-pass filter. Cells were imaged in 3D (with a 1- to 2-μm z-step) at multiple locations in both hypocotyl and root. They were left on the slide to induce hypoxia and reimaged ~60 min later, when speckled patterns had formed. After that, the hypoxia stress was relieved by removing the plants from the slide and allowing them to recover in MS media for 3 h and then reimaged.

*Arabidopsis* culture cells were embedded in 2% agarose and placed into the modified gas-permeable biochamber, where the gas-permeable membrane could be blocked to induce hypoxia or exposed to air. Cells were imaged in 3D (with a 1- to 2-μm z-step) at multiple locations under nonstressed conditions. The membrane was then blocked to induce hypoxia stress, and the stressed cells were then reimaged after 60 min. To relieve the hypoxia stress, the membrane was then allowed to breathe again allowing the cells to recover and reimaged after 30 min.

### FRAP Analysis

FRAP experiments were performed using a Leica SP2 laser scanning confocal microscope (Leica Microsystems) equipped with a 100-mW argon ion laser. The Leica MicroLab FRAP module was used in "Flymode" to bleach an x-line in one direction and then acquire data in the revere direction of the scan to minimize the time delay between the bleach and the first post image. The kinetics of GFP-eIF4A-III was studied in both Col-0 cells and *Arabidopsis* seedlings.

Col-0 cells in exponential phase of the culture (within 2 to 5 d of subculturing in fresh media) transiently expressing GFP-eIF4A-III were placed in a gas-permeable chamber (nonstress conditions) or on a standard microscope slide (induces hypoxia stress). Cells were observed using a ×40 oil immersion objective, zoom × 4, 512 × 32 pixels, 400 Hz, and imaged (pre- and postbleaching) using 3% of the 488-nm line from an argon ion laser running at 75% power; emission was captured from a 505- to 555-nm window with an open detector pinhole. Ten data points were acquired within 3 to 4 s to measure prebleaching intensity in a selected area. A small circular area (3 μm in diameter) was photobleached using 100% of 457-, 477-, and 488-nm lines from the argon ion laser with five iterations. The bleaching scan lasted ~1.8 s and was immediately followed by imaging scans at the line level, with only a few milliseconds delay. Images were taken at 360-ms intervals for 50 s when the maximal recovery of the signal was observed.

*Arabidopsis* seedlings 3 to 5 d old stably expressing GFP-eIF4A-III were placed in a gas-permeable chamber (nonstress conditions) or on a

standard microscope slide (induces hypoxia stress). Seedlings were observed using a ×63 oil immersion objective, zoom × 4, 512 × 64 pixels, 1000 Hz, and imaged (pre- and postbleaching) using 3% of the 488-nm line from an argon ion laser running at 100% power; emission was captured from the 505- to 555-nm window with an open detector pinhole. Twenty data points were acquired within 3 to 4 s to measure prebleaching intensity in a selected area. A small circular area (3 μm in diameter) was photobleached using 100% of 457-, 477-, and 488-nm lines from the argon ion laser with two iterations. The bleaching scan lasted ~0.328 s and was immediately followed by imaging scans at the line level, with only a few milliseconds delay. Images were taken at 164-ms intervals for 25 s when the maximal recovery of the signal was observed.

The intensities of the signal were background-normalized to produce relative fluorescence intensity data. Average values of relative fluorescence intensity recovery from 10 independent FRAP experiments for each subnuclear compartment were used for quantitative data analysis of GFP-eIF4A-III kinetics in nucleoplasm, nucleolus, and speckles. Formal kinetic parameters of recovery were estimated using curve fitting software TableCurve 2D (v 5.01 for Windows; SYSTAT Software). Average background-normalized recovery data for nucleoplasm, nucleolus, and speckles from 10 independent experiments for each subnuclear compartment were fitted into exponential model curves using an equation of one-phase exponential formation/ association, $Y = a^*(1 - \exp^{(-b^*T)})$, where a is the final level of signal recovery (proportion of initial relative intensity), T is time in seconds, and b is the rate of recovery constant. Half-time of fluorescence recovery was calculated as $T_{1/2} = \ln 2/b$.

### Respiratory Inhibitor Studies

The eIF4A-III plants were treated with sodium azide (1 and 100 mM) for a minimum time of 30 min before imaging. Plants were visualized using a VisiTech VoxCell QLC100 spinning disc confocal microscope (VisiTech International) with ×40 oil immersion objective. GFP was excited using the 488-nm laser line from an argon ion laser, and its emission was collected through 500- to 550-nm band-pass filter and detected on a Hamamatsu Orca ER cooled CCD camera.

### Proteasome Inhibitor Studies

Transiently transformed cells in the exponential phase (3 to 4 d after dilution/transformation by *A. tumefaciens*) were diluted 1:3 by fresh AT media for Col-0 cells (see above), dispensed as 2-mL aliquots in six-well plates, and MG132 proteasome inhibitor was added for a final concentration of 100 μM. The plates were sealed by air-permeable Micropore tape and placed in the dark shaker/incubator at 25°C and 150 rpm. In a pilot experiment, imaging was performed at 1-h intervals to determine the time required for redistribution of the signal in response to a treatment. The redistribution was observed after 3 h of incubation and remained stable for at least next 2 h; therefore, a time interval 3 to 5 h of treatment was used for taking samples for imaging and cell counting. To avoid interference of the inhibitor assays with hypoxia, cell counts were performed on each slide for not longer than 10 min. Nuclei were counted and their staining pattern assigned as nucleoplasmic, nucleolus, nucleolus plus speckles, or speckles. The results were subjected to statistical analysis by comparing cell counts of localization types by a generalized linear model with a log link and Poisson error and estimating significance based on approximate F probabilities from appropriate deviance ratios.

### RNA Extraction and RT-PCR Splicing Analysis

RNA and RT-PCR was as described previously (Simpson et al., 2008). In summary, total RNA was extracted from 50 to 100 mg of ground azide-treated tissue using the RNeasy plant mini RNA isolation kit (Qiagen) followed by first-strand cDNA synthesis on 5 μg of total RNA using "Ready to go-you prime" first-strand beads (Amersham) and oligo $d(T)^{18}$ according to the manufacturer's instructions. The reverse transcription reaction was diluted to a final volume of 100 μL and 1 μL aliquoted into a 96-well reaction plate along with 1× PCR buffer (10 mM Tris-HCl, pH 8.3, 50 mM KCl, and 3 mM $MgCl_2$), 0.2 mM dATP, dCTP, dGTP, and dTTP (Promega), 1.5 μM of each of the gene-specific primers (see Supplemental Table 3 online), and Taq DNA Polymerase (Roche). The PCR reaction was performed for 24 cycles, which we have previously shown to be in the linear amplification range for a number of different genes with different expression levels (Simpson et al., 2008). The gene-specific primers amplify all transcripts in the particular region of the gene, allowing their relative abundance to be measured. To identify transcripts with retained introns on the ABI3730, the primers were designed across two to four introns, and the forward primer was labeled with 6-carboxyfluoresceine to visualize the RT-PCR products.

One microliter of each RT-PCR reaction was separated on a 3730 DNA Analyzer (Applied Biosystems) and peak data collected and analyzed using Genemapper software (Applied Biosystems). The relative peak areas of RT-PCR products representing fully spliced transcripts, transcripts with retained introns, and other alternatively spliced transcripts if detected were extracted and the ratio of products calculated. For accurate measurement of intron retention in the azide treatments, RNA from three biological samples was used and mean AS efficiencies with standard errors were calculated.

### Accession Numbers

Sequence data from this article can be found in the Arabidopsis Genome Initiative or GenBank/EMBL databases under the following accession numbers *Arabidopsis* eIF4A-III (NP_188610.1), *H. sapiens* eIF4A-III (NP_055555.1), *M. musculus* eIF4A-III (NP_619610.1), *D. rerio* eIF4A-III (NP_957372.1), *C. elegans* eIF4A-III (NP_491703.1), *D. melanogaster* eIF4A-III (NP_649788.2), *Arabidopsis* RNPS1/SR45 (NC_003070.6), *Arabidopsis* FIBRILLARIN 1 (NC_003076.5), *Arabidopsis* CypRS64 (NC_003074.5), *Arabidopsis* Y14 (NP_564591), *Arabidopsis* ALY4 (NP_001078676.1), and *Arabidopsis* MLN51 (NP_565226).

### Supplemental Data

The following materials are available in the online version of this article.

**Supplemental Figure 1.** Yeast Two-Hybrid Screen Showing Reciprocal Interactions between EJC Components.

**Supplemental Figure 2.** Dynamics of Speckle Formation in Col-0 Culture Cells Transiently Expressing GFP-EIF4AIII in a Gas-Permeable Chamber with Small Volume.

**Supplemental Figure 3.** RT-PCR Analysis of Intron Retention Events.

**Supplemental Table 1.** Intron Retention Events Analyzed by RT-PCR.

**Supplemental Table 2.** Primers Used in This Study.

**Supplemental Table 3.** Primers Used to Examine Intron Retention Events.

**Supplemental Movie 1.** Dynamics of Speckle Formation in Col-0 Culture Cells Transiently Expressing GFP-eIF4AIII, Placed on a Microscope Glass Slide with a Cover Slip.

**Supplemental Movie 2.** Dynamics of Speckle Formation in Col-0 Culture Cells Transiently Expressing eIF4A-III, in a Gas-Permeable Chamber with Small Volume.

**Supplemental Movie 3.** Dynamics of eIF4A-III in *Arabidopsis* Roots Placed in a Chamber with Adequate Aeration.

**Supplemental Movie 4.** Dynamics of eIF4A-IIIin *Arabidopsis* Roots Placed in a Chamber with Hypoxic Conditions.

**Supplemental Movie 5.** Time-Lapse Movie of a Typical FRAP Experiment Performed on Nucleoplasmic Fraction.

**Supplemental Movie 6.** Time-Lapse Movie of a Typical FRAP Experiment Performed on Nucleolar Fraction.

**Supplemental Movie 7.** Time-Lapse Movie of a Typical FRAP Experiment Performed on Speckle Fraction.

**Supplemental Data Set 1.** Text File Corresponding to the Alignment in Figure 1.

## ACKNOWLEDGMENTS

We thank Z. Lorkovic and A. Barta for kindly providing pCypRS64-GFP plasmid and V. Mikitova for advice and help with yeast two-hybrid assays. This work was supported by the Biotechnology and Biological Sciences Research Council of the UK (Grant BBS/B/13519) to the John Innes Centre, the Scottish Government Rural and Environment Research and Analysis Directorate (Grant SCR/909/03) to the Scottish Crop Research Institute, and by the European Alternative Splicing Network of Excellence (Contract 518238).

Received May 5, 2008; revised March 12, 2009; accepted April 29, 2009; published May 12, 2009.

## REFERENCES

**Alastalo, T.P., Hellesuo, M., Sandqvist, A., Hietakangas, V., Kallio, M., and Sistonen, L.** (2003). Formation of nuclear stress granules involves HSF2 and coincides with the nucleolar localization of Hsp70. J. Cell Sci. **116:** 3557–3570.

**Ali, G.S., and Reddy, A.S.** (2006). ATP, phosphorylation and transcription regulate the mobility of plant splicing factors. J. Cell Sci. **119:** 3527–3538.

**Andersen, C.B., Ballut, L., Johansen, J.S., Chamieh, H., Nielsen, K.H., Oliveira, C.L., Pedersen, J.S., Seraphin, B., Le Hir, H., and Andersen, G.R.** (2006). Structure of the exon junction core complex with a trapped DEAD-box ATPase bound to RNA. Science **313:** 1968–1972.

**Ares, M., Jr., and Proudfoot, N.J.** (2005). The spanish connection: transcription and mRNA processing get even closer. Cell **120:** 163–166.

**Bailey-Serres, J., and Chang, R.** (2005). Sensing and signalling in response to oxygen deprivation in plants and other organisms. Ann. Bot. (Lond.) **96:** 507–518.

**Baldin, V., Militello, M., Thomas, Y., Doucet, C., Fic, W., Boireau, S., Jariel-Encontre, I., Piechaczyk, M., Bertrand, E., Tazi, J., and Coux, O.** (2008). A novel role for PA28{gamma}-proteasome in nuclear speckle organization and SR protein trafficking. Mol. Biol. Cell **19:** 1706–1716.

**Ballut, L., Marchadier, B., Baguet, A., Tomasetto, C., Seraphin, B., and Le Hir, H.** (2005). The exon junction core complex is locked onto RNA by inhibition of eIF4AIII ATPase activity. Nat. Struct. Mol. Biol. **12:** 861–869.

**Bono, F., Ebert, J., Lorentzen, E., and Conti, E.** (2006). The crystal structure of the exon junction complex reveals how it maintains a stable grip on mRNA. Cell **126:** 713–725.

**Branco-Price, C., Kaiser, K.A., Jang, C.J., Larive, C.K., and Bailey-Serres, J.** (2008). Selective mRNA translation coordinates energetic and metabolic adjustments to cellular oxygen deprivation and reoxygenation in *Arabidopsis thaliana*. Plant J. **56:** 743–755.

**Campbell, R.E., Tour, O., Palmer, A.E., Steinbach, P.A., Baird, G.S., Zacharias, D.A., and Tsien, R.Y.** (2002). A monomeric red fluorescent protein. Proc. Natl. Acad. Sci. USA **99:** 7877–7882.

**Carmo-Fonseca, M., Mendes-Soares, L., and Campos, I.** (2000). To be or not to be in the nucleolus. Nat. Cell Biol. **2:** E107–E112.

**Chan, C.C., Dostie, J., Diem, M.D., Feng, W., Mann, M., Rappsilber, J., and Dreyfuss, G.** (2004). eIF4A3 is a novel component of the exon junction complex. RNA **10:** 200–209.

**Clough, S.J., and Bent, A.F.** (1998). Floral dip: A simplified method for Agrobacterium-mediated transformation of *Arabidopsis thaliana*. Plant J. **16:** 735–743.

**Collier, S., Pendle, A., Boudonck, K., van Rij, T., Dolan, L., and Shaw, P.** (2006). A distant coilin homologue is required for the formation of cajal bodies in Arabidopsis. Mol. Biol. Cell **17:** 2942–2951.

**Dhalia, R., Marinsek, N., Reis, C.R., Katz, R., Muniz, J.R., Standart, N., Carrington, M., and de Melo Neto, O.P.** (2006). The two eIF4A helicases in *Trypanosoma brucei* are functionally distinct. Nucleic Acids Res. **34:** 2495–2507.

**Geigenberger, P.** (2003). Response of plant metabolism to too little oxygen. Curr. Opin. Plant Biol. **6:** 247–256.

**Hochachka, P.W., Buck, L.T., Doll, C.J., and Land, S.C.** (1996). Unifying theory of hypoxia tolerance: Molecular/metabolic defense and rescue mechanisms for surviving oxygen lack. Proc. Natl. Acad. Sci. USA **93:** 9493–9498.

**Kohli, D.K., and Bachhawat, A.K.** (2003). CLOURE: Clustal Output Reformatter, a program for reformatting ClustalX/ClustalW outputs for SNP analysis and molecular systematics. Nucleic Acids Res. **31:** 3501–3502.

**Koroleva, O.A., Tomlinson, M.L., Leader, D., Shaw, P., and Doonan, J.H.** (2005). High-throughput protein localization in Arabidopsis using Agrobacterium-mediated transient expression of GFP-ORF fusions. Plant J. **41:** 162–174.

**Lamond, A.I., and Earnshaw, W.C.** (1998). Structure and function in the nucleus. Science **280:** 547–553.

**Lamond, A.I., and Spector, D.L.** (2003). Nuclear speckles: A model for nuclear organelles. Nat. Rev. Mol. Cell Biol. **4:** 605–612.

**Lejeune, F., and Maquat, L.E.** (2005). Mechanistic links between nonsense-mediated mRNA decay and pre-mRNA splicing in mammalian cells. Curr. Opin. Cell Biol. **17:** 309–315.

**Li, Q., Imataka, H., Morino, S., Rogers, G.W., Jr., Richter-Cook, N.J., Merrick, W.C., and Sonenberg, N.** (1999). Eukaryotic translation initiation factor 4AIII (eIF4AIII) is functionally distinct from eIF4AI and eIF4AII. Mol. Cell. Biol. **19:** 7336–7346.

**Lorkovic, Z.J., and Barta, A.** (2004). Compartmentalization of the splicing machinery in plant cell nuclei. Trends Plant Sci. **9:** 565–568.

**Lorkovic, Z.J., Lopato, S., Pexa, M., Lehner, R., and Barta, A.** (2004). Interactions of Arabidopsis RS domain containing cyclophilins with SR proteins and U1 and U11 small nuclear ribonucleoprotein-specific proteins suggest their involvement in pre-mRNA splicing. J. Biol. Chem. **279:** 33890–33898.

**Ma, X.M., Yoon, S.O., Richardson, C.J., Julich, K., and Blenis, J.** (2008). SKAR links pre-mRNA splicing to mTOR/S6K1-mediated enhanced translation efficiency of spliced mRNAs. Cell **133:** 303–313.

**Maquat, L.E.** (2004). Nonsense-mediated mRNA decay: Splicing, translation and mRNP dynamics. Nat. Rev. Mol. Cell Biol. **5:** 89–99.

**Misteli, T.** (2005). Concepts in nuclear architecture. Bioessays **27:** 477–487.

**Misteli, T., and Spector, D.L.** (1998). The cellular organization of gene expression. Curr. Opin. Cell Biol. **10:** 323–331.

**Noble, C.G., and Song, H.** (2007). MLN51 stimulates the RNA-helicase activity of eIF4AIII. PLoS One **2:** e303.

**Owttrim, G.W., Mandel, T., Trachsel, H., Thomas, A.A., and Kuhlemeier, C.** (1994). Characterization of the tobacco eIF-4A gene family. Plant Mol. Biol. **26:** 1747–1757.

**Park, N.I., and Muench, D.G.** (2007). Biochemical and cellular characterization of the plant ortholog of PYM, a protein that interacts with the exon junction complex core proteins Mago and Y14. Planta **225:** 625–639.

**Pederson, T.** (1998). Thinking about a nuclear matrix. J. Mol. Biol. **277:** 147–159.

**Pendle, A.F., Clark, G.P., Boon, R., Lewandowska, D., Lam, Y.W., Andersen, J., Mann, M., Lamond, A.I., Brown, J.W., and Shaw, P.J.** (2005). Proteomic analysis of the Arabidopsis nucleolus suggests novel nucleolar functions. Mol. Biol. Cell **16:** 260–269.

**Pengelley, S.C., Chapman, D.C., Mark Abbott, W., Lin, H.H., Huang, W., Dalton, K., and Jones, I.M.** (2006). A suite of parallel vectors for baculovirus expression. Protein Expr. Purif. **48:** 173–181.

**Rackham, O., and Brown, C.M.** (2004). Visualization of RNA-protein interactions in living cells: FMRP and IMP1 interact on mRNAs. EMBO J. **23:** 3346–3355.

**Raska, I., Shaw, P.J., and Cmarko, D.** (2006). Structure and function of the nucleolus in the spotlight. Curr. Opin. Cell Biol. **18:** 325–334.

**Rossignol, P., Collier, S., Bush, M., Shaw, P., Doonan, J.H.** (2007). Arabidopsis POT1A interacts with TERT-V(I8), an N-terminal splicing variant of telomerase. J. Cell Sci. **120:** 3678–3687.

**Segui-Simarro, J.M., Testillano, P.S., and Risueno, M.C.** (2003). Hsp70 and Hsp90 change their expression and subcellular localization after microspore embryogenesis induction in *Brassica napus* L. J. Struct. Biol. **142:** 379–391.

**Shav-Tal, Y., and Singer, R.H.** (2005). RNA localization. J. Cell Sci. **118:** 4077–4081.

**Shaw, P.J., and Jordan, E.G.** (1995). The nucleolus. Annu. Rev. Cell Dev. Biol. **11:** 93–121.

**Shibuya, T., Tange, T.O., Sonenberg, N., and Moore, M.J.** (2004). eIF4AIII binds spliced mRNA in the exon junction complex and is essential for nonsense-mediated decay. Nat. Struct. Mol. Biol. **11:** 346–351.

**Shibuya, T., Tange, T.O., Stroupe, M.E., and Moore, M.J.** (2006). Mutational analysis of human eIF4AIII identifies regions necessary for exon junction complex formation and nonsense-mediated mRNA decay. RNA **12:** 360–374.

**Simpson, C.G., Fuller, J., Maronova, M., Kalyna, M., Davidson, D., McNicol, J., Barta, A., and Brown, J.W.** (2008). Monitoring changes in alternative precursor messenger RNA splicing in multiple gene transcripts. Plant J. **53:** 1035–1048.

**Stutz, F., and Izaurralde, E.** (2003). The interplay of nuclear mRNP assembly, mRNA surveillance and export. Trends Cell Biol. **13:** 319–327.

**Tange, T.O., Nott, A., and Moore, M.J.** (2004). The ever-increasing complexities of the exon junction complex. Curr. Opin. Cell Biol. **16:** 279–284.

**Tillemans, V., Dispa, L., Remacle, C., Collinge, M., and Motte, P.** (2005). Functional distribution and dynamics of Arabidopsis SR splicing factors in living plant cells. Plant J. **41:** 567–582.

**Tillemans, V., Leponce, I., Rausin, G., Dispa, L., and Motte, P.** (2006). Insights into nuclear organization in plants as revealed by the dynamic distribution of Arabidopsis SR splicing factors. Plant Cell **18:** 3218–3234.

**Vayda, M.E., Shewmaker, C.K., and Morelli, J.K.** (1995). Translational arrest in hypoxic potato tubers is correlated with the aberrant association of elongation factor EF-1 alpha with polysomes. Plant Mol. Biol. **28:** 751–757.